Title:
Identification and characterization of a stress-responsive *TAS3*-derived tasiRNA in melon

Running title:
tasiRNAs and stress response in melon

Corresponding author:
gustavo.gomez@csic.es

Subject area:
Environment and stress response

Number of colour figures:
5

Number of tables:
1

Number of supplementary figures:
3

Number of supplementary tables:
6

Identification and characterization of a stress-responsive *TAS3*-derived tasiRNA in melon

Luis Cervera-Seco[1], María Carmen Marques[1], Alejandro Sanz-Carbonell[1], Joan Marquez-Molins[1], Alberto Carbonell[2], José-Antonio Daròs[2] and Gustavo Gomez[1*].

[1] Institute for Integrative Systems Biology (I2SysBio), Consejo Superior de Investigaciones Científicas (CSIC) - Universitat de València (UV), Parc Científic, Cat. Agustín Escardino 9, 46980 Paterna, Spain.

[2] Instituto de Biología Molecular y Celular de Plantas (IBMCP), Consejo Superior de Investigaciones Científicas (CSIC) - Universitat Politècnica de València, CPI 8E, Av. de los Naranjos s/n, 46022 Valencia, Spain.

[*] *Corresponding author*: E-mail: gustavo.gomez@csic.es

Running title: tasiRNAs and stress response in melon

ABSTRACT

Small interfering RNAs (siRNA) are key regulators of gene expression that play essential roles in diverse biological processes. *Trans*-acting siRNAs (tasiRNAs) are a class of plant-endogenous siRNAs that lead the cleavage of non-identical transcripts. TasiRNAs are usually involved in fine-tuning development. However, increasing evidence supports the notion that these plant-specific molecules may be involved in (abiotic and biotic) stress response. Melon (*Cucumis melo*) is a crop of great economic importance extensively cultivated in semiarid regions frequently exposed to changing environmental conditions that limit its productivity. However, knowledge of the precise role of siRNAs in general, and of tasiRNAs in particular, in regulating the response to adverse environmental conditions is limited. Here we provide the first comprehensive analysis of computationally inferred tasiRNAs responsive to two biotic (viroid-infection) and abiotic (cold treatment) stress conditions in melon. First, the *TAS* candidates (*cmTAS*) predicted from small RNA sequencing data were characterized according to their chromosome localization and expression pattern in response to stress. Second, the functional activity of *cmTAS* genes was validated by transcript quantification and degradome assays of the tasiRNA precursors and their predicted targets. Finally, the functionality of a representative *cmTAS3*-derived tasiRNA was confirmed by transient assays showing the cleavage of *ARF* target transcripts.

Keywords:
Cucurbitaceae, ncRNAs, Plant-environment interactions, Regulation of the stress-response in crops, RNA silencing, small RNAs in melon,

Introduction

Adverse environmental conditions, either of both biotic and/or abiotic origin, cause severe productivity constrains in major crops leading to important economic losses worldwide (Sunkar et al. 2007, Calanca, 2017). As sessile organisms, plants have developed various protective mechanisms to counteract stress situations. As a general strategy, gene expression is fine-tuning regulated to assist the physiological changes necessary to ensure plant adaptation to changing environments (Zhang 2015, Zhu 2016, Banerjeeab et al. 2017, Bielach et al. 2017).

Small regulatory RNAs (21–24 nt in size) are key regulators of gene expression in plants, playing essential roles in diverse biological processes (Bologna and Voinnet, 2014, Borges and Martienssen, 2015, Martinez and Köhler, 2017). Upon production, small RNAs (sRNAs) are loaded into their effector protein named ARGONAUTE (AGO), and guide it to recognize target RNAs or DNA through sequence complementarity (Yu et al. 2017, Carbonell, 2017). AGO/sRNA complexes negatively modulate gene expression at both transcriptional and post-transcriptional levels, by directing DNA methylation or histone modification, and through target RNA cleavage or translational inhibition, respectively (D'Ario et al. 2017, Yang et al. 2018).

Endogenous plant sRNAs are classified primarily according to their initial processing source. The small RNAs derived from double-stranded RNA (dsRNA) precursors are known as small interfering RNAs (siRNAs), and sRNAs arising from single-stranded self-complementary hairpin structures are named microRNAs (miRNAs) (Axtell, 2013). While increasing evidences support the notion that miRNAs act as master regulators of the plant responses to environmental changes (Zhang 2015, Islam et al. 2018, Sunkar et al. 2012, Kumar, 2014, Sanz-Carbonell et al. 2019), the role of siRNAs in these processes remains obscure.

Based on their origin, biogenesis and/or mode of action, endogenous siRNAs can be further classified into phased siRNAs (pha-siRNAs), heterochromatic siRNAs (hc-siRNAs), and natural antisense siRNAs (nat-siRNAs) (Yu et al. 2017, Axtell, 2013, Shriram et al. 2016).

When a plant transcript is targeted by a miRNA, it can generate multiple siRNAs in a phased pattern relative to the miRNA cleavage site, these small RNAs are termed phasiRNAs (Deng et al. 2018, Fei et al., 2013). If the miRNA-sliced transcript is a noncoding RNA, it generates a subset of phasiRNAs known as trans-acting siRNAs (tasiRNAs) that target *in trans* RNAs distinct from those from which they derive; hence the term *trans*-acting siRNAs (Deng et al. 2018, Allen et al. 2005, Axtell 2013).

In the tasiRNA biogenesis model, a specific miRNA directs the AGO-dependent cleavage of Pol II-dependent *TAS* transcripts. Next a protein complex that includes RNA-dependent RNA polymerase 6 (RDR6), suppressor of gene silencing 3 (SGS3) and double-stranded RNA binding 4 (DRB4) (Adenot et al. 2006, Fukunaga and Doudna, 2009), is recruited to one of the cleavage fragments to generate a dsRNA. This dsRNA is sequentially processed by DCL4 into 21-nucleotide (nt) tasiRNA duplexes in register with the miRNA-guided cleavage site (Allen et al. 2005, Axtell et al. 2006). One strand of the tasiRNA duplex is selectively loaded into an AGO protein according to the sRNA 5′ nt, or to other sequence/structural elements of sRNA, the sRNA duplex or the PIWI domain (Zhang et al. 2014, Mi et al. 2008, Montgomery et al. 2008, Takeda et al. 2008, Zhu et al. 2011).

TasiRNAs were initially identified in *Arabidopsis thaliana* (arabidopsis), where four gene families, *TAS1*, *TAS2*, *TAS3*, and *TAS4*, have been described. The processing of *TAS1* and *TAS2* precursors in arabidopsis is initiated by miR173 cleavage; while *TAS3* and *TAS4* biogenesis is triggered by miR390 and miR828, respectively (Allen et al. 2005, Howell et al. 2007, Allen and Howell, 2010). TasiRNAs have been characterized across a wide range of plant species, from the moss *Physcomitrella patens* (Axtell et al. 2006, Talmor-Neiman et al. 2006, Arif et al. 2012) to higher plants like rice, maize, pine and tomato (Williams et al. 2005, Axtell et al. 2006, Heisel et al. 2008, Johnson et al. 2009, Wu et al. 2017), suggesting that these regulatory RNAs form part of a common ancient pathway in plants. Although they have been described as regulators of plant developmental processes (Chitwood et al. 2009, Marin et al. 2010, Fei et al. 2013), tasiRNAs may also be involved in abiotic and biotic stress responses (Hsieh et al. 2009, Li et al. 2012, Luo et al 2012, Wu et al. 2017). Among plant *TAS* genes, the most widely studied is *TAS3*

whose transcript bears two target sites of miR390, generating tasiRNAs via the so-called "*two-hit*" mechanism (Axtell et al. 2006). Very recently, however, it has been shown that –at least in arabidopsis- a single miR390 targeting event is sufficient for *TAS3*-based tasiRNA biogenesis (de Felippes et al. 2017).

Melon (*Cucumis melo*) is a crop of great economic relevance. It is extensively cultivated in semi-arid regions frequently exposed to changing environmental conditions that affects its production (Wei et al. 2013). The recent development of molecular tools such as EST collections (Clepet et al. 2011), TILLING platforms (González et al. 2011), and genome sequencing and annotation (Garcia-Mas et al. 2012, Ruggieri et al. 2018), has favored the emergence of melon as a valuable experimental system to conduct significant agricultural-related research focused on development (Wu et al. 2018) or response to stress (Bustamante et al. 2018, Sanz-Carbonell et al. 2019). Although, a melon genome region containing two predicted miR390 targets sites able to generate phased-sRNAs and reminiscent to *TAS3* genes was previously identified computationally (Gonzalez-Ibeas et al. 2011), the role that siRNAs in general and tasiRNAs in particular play in the regulation of the response to stress in melon plants remains in a conundrum.

In order to gain insight into stress-responsive *TAS*-derived tasiRNA in melon, potential TAS loci (*CmTAS*) were computationally inferred. Next, we located these *cmTAS* in the melon chromosome and analyzed their expression patterns in response to stress. Finally, we functionally validated *CmTAS* genes by analysis of melon degradome and transient assays in *Nicotiana benthamiana*. The results shown here indicate that the processing of *TAS3*-derived tasiRNAs in melon is a functional process related to environmental conditions.

Results

Prediction and annotation of melon TAS loci

For genome-wide detection of putative *TAS* loci in melon, the *TASI-PREDICTION* tool included in the *UEA small RNA Workbench* (v.4.4) was employed using as input data the reads recovered from sRNA libraries obtained from melon plants exposed to seven biotic and abiotic stress conditions (Bustamante et al. 2018, Sanz-Carbonell et al. 2019) and the melon genome sequence (Version 3.5.1)

[47]. The software parameters established for a more robust prediction of phased siRNAs in melon are detailed in the Materials and Methods section. In all, 895 regions were identified as being potential phasi-generators loci in the melon genome (**Table S1**).

Then these potential *TAS* precursors were filtered according to the following parameters: *i*) homology with known *TAS* loci and *ii*) ≥5 phased sequences identified (at least one in both senses).

We identified four melon genomic regions highly homologous to known *TAS* genes: one (*TAS-Cmel779*) matching arabidopsis *TAS2* and three (*TAS-Cmel028*, *TAS-Cmel735*, and *TAS-Cmel737*) homologous to *TAS3* precursors identified in *Wolffia arrhiza, Solanum demissum,* and *Oryza sativa*, respectively (**Table S2**). Two of the potential *TAS* precursors (*TAS-Cmel779* and *TAS-Cmel028*) were discarded because of the low number (three) of phased sequences recovered and the shortness (32 nt) of the homologous region, respectively. The two selected potential *TAS3* loci (*TAS-Cmel735* and *TAS-Cmel737*) were localized in chromosome 11. Regarding the number of phased sRNAs matching predicted *TAS* regions, *TAS-Cmel735* with 23 sequences (12 sense and 11 antisense) was the most highly represented.

To increase the specter of our search, potential phasiRNA precursor non homologous to known *TAS* genes were reanalyzed following a strategy similar to the previously described to identify phased siRNAs in grapevine (Zhang et al 2012). First, we retrieved the genomic region containing the predicted TAS and an additional 100 nt either to its left or right. Next, we searched for predicted regions between melon miRNAs and the retrieved genomic sequence using psRNATarget. As a final step, we validated the predicted miRNA cleavage position analyzing our degradome dataset. Under this analysis condition we identify an additional potential *TAS* loci identified as *TAS-Cmel087* sliced in their 5´region by miR828, reminiscent to *TAS4* in arabidopsis. However this predicted precursors was discarded because of the low number (four) of phased sequences recovered (Table S2). The process employed to identify potential *TAS* loci in melon is represented in **Figure S1**.

The actual sequences of the both, *Cmel735* and *Cmel737,* predicted *TAS* loci recovered from the melon genome were confirmed by sequencing of PCR-

amplified products (**Figure S2A**). Finally, the presence of transcripts derived from these predicted *TAS* loci was validated by RT-PCR assays and the subsequent sequencing of the amplified products (**Figure S2B**).

Identification and validation of potential tasiRNA triggers

Considering that the "*two-hit*" mechanism (Axtell et al. 2006) is the commonest processing mechanism to trigger *TAS3* derived tasiRNAs in plants, as last filtering criteria we considered as potential *TAS* precursors only those containing the double recognition sites for the melon miRNAs found in the miRbase. To identify miRNA target sites in these potential *TAS* precursors, miRNA binding site prediction was performed using the *psRNAtarget* server (Dai et al. 2018). As shown in **Table S2,** two miR390 target sites for melon miRNAs recovered from the miRBase were predicted for both *TAS-Cmel735* and *TAS-Cmel737*. As expected (the functional complex *TAS3*/miR390 is highly conserved in plants) (Xia et al. 2017), the two predicted *cmTAS3* precursors included miR390 target sites. For *TAS-Cmel735* and *TAS-Cmel737*, the miR390 target sites were located between the positions 24043012-24042992 (cut at 5´) and 24042821-24042801 (cut at 3´), and between positions 28041083-28041103 (5´) and 28041335-28041355 (3´) of chromosome 11, respectively (Table S2). *TAS-Cmel 735* (212 nt) was relatively short compared to the *TAS-Cmel 737* (273 nt), resembling the previously observed in apple and strawberry when two *TAS3* families encoding length (*TAS3-L)* and short (*TAS3-S*) transcripts, respectively, were described (Xia et al, 2012, Xia et al. 2015).

Predicted miRNA-mediated processing of *TAS-Cmel735* and *TAS-Cmel737* precursors was evaluated by 5'-RLM-RACE assays. The results indicated that only remnants derived from the canonical (cleavage position between nucleotides 10 and 12 in relation to the 5'-end of the miRNAs) cut of *TAS-Cmel735* guided by miR390 in both 5´ and 3´ regions were recovered from our dataset (**Figure 1 and Figure S3A - B**). According to the number of normalized reads recovered from degradome assay matching onto both 5´ and 3´ regions [2 reads per million (RPM) and 2734 RPM, respectively], it was possible to infer that the 3´ region was the most highly processed and could possibly act as the starting point for the sequential processing of *TAS-Cmel735* (potential *TAS3*) in melon. In addition,

and as expected, when the 21 nt-long sRNAs recovered from the melon sRNAs libraries were plotted onto the potential *TAS-Cmel735* genomic region, all analyzed sequences matched exclusively the area comprised within both miR390 target-sites, which according to the biogenesis model for tasiRNA-production, constitutes the external limits of the miRNA-processed *TAS* precursor (**Figure 2A**). In coincidence with the previously described for *TAS3-S* family in other dicotyledonous species (Xia et al., 2015), the residual miR390-silicing of the TAS-precursor in their 5´ region was able to trigger the production of phased siRNAs (Figure 2C).

Contrarily to the expected, when a similar analysis was performed onto the *TAS-Cmel737* transcript (that according our degradome data is not sliced by miR390), all analyzed sRNA sequences matched exclusively the area comprised within both computationally inferred miR390 target-sites and exhibit high accumulation of miR390-related phased siRNAs (Figure S3C).

Determination of TAS3-derived tasiRNAs targets in melon

To elucidate the basis of the regulatory pathways modulated by the predicted *cmTAS3*, we analyzed the existing relationship between the phased siRNAs recovered from our data set and their intended targets. According to the miR390-guided cleavage site validated by 5'-RLM-RACE in the *TAS-Cmel735*, nine potential 21 nt-long tasiRNAs were predicted to be produced from the processed *TAS3* precursor in melon (**Figure 2B**). These in-phase siRNAs were named 5'D1[+] to 5'D9[+], starting from the miR390 cleavable target site identified in the 3´region of the potential *TAS* transcript. In addition, we also analyze potential phased siRNAs arising from the unprocessed miR390 target position predicted in the transcripts derived from *TAS-Cmel737* (Figure S3D).

On the basis of psRNA target results (considering only transcripts with well established biological function), the lower expectative values (expect. ≤1) were obtained for three melon transcripts that were predicted as candidates to be negatively regulated by *TAS-Cmel735*-derived tasiRNA 5'D6[+] and *TAS-Cmel737*-derived tasiRNA 5'D7[+] and 5'D8[+] (**Table S3**). Consistently with the tasiRNA targets established in arabidopsis (Xia et al. 2017), mRNAs related to AUXIN RESPONSE FACTORS (ARF) family (ARF2, ARF3 and ARF4) were

identified as potential targets for *TAS3*-derived siRNAs (tasiARF) activity. As observed in diverse plant species, two recognition sites for tasiARF-AGO activity were identified in *ARF* transcripts (**Table S3**). Like the commonly described for *TAS3-L* family, two tasiARFs were derived from the *TAS-Cmel737* transcript. In contrast, *TAS-Cmel735* transcript encodes only one tasiARF, sharing also structural resemblance with *TAS3-S* family (Xia et al. 2012, Xia et al. 2017).

To validate the functionality of the predicted tasiRNA-target interactions, we analyzed by 5'-RLM-RACE the processing of the transcripts expected to be regulated by tasiARF in melon. As shown in **Figure 3,** for the ARF3 melon transcript, we detected sequences-remnants coincident with those expected for transcripts sliced via *TAS3*-derived tasiRNA-guided AGO activity in the two predicted target sites. In contrast, only one of the two cleavage positions estimated by psRNA-target for the tasiRNA-ARF4 interaction was validated by the degradome assays (**Figure 3**). Finally sequences-remnants coincident with the expected processing of ARF2 by *TAS-Cmel737 derived* tasiRNA 5'D7[+] and 5'D8[+] were also detected (Figure 3).

In vivo validation of the interplay tasiARF/target.

To provide further evidence for the biological activity of the *TAS3*-derived tasiARF identified in melon, the tasiARF derived from *TAS-Cmel735* transcript (*TAS3-S*) was expressed from a functional syn-tasiRNA vector including a modified *TAS1c* precursor from arabidopsis (Carbonell et al. 2014). The resulting syn-tas-cm*TAS*3 construct is shown in **Figure 4A**. As a functional reporter of tasiRNA-activity, we used a construct containing a common region of ARF3 and ARF4 cDNA consisting of the predicted tasiARF target site (AGGUCUUGCAAGGUCAAGAAA) fused to the 3´ end of the yellow fluorescent protein (YFP) mRNA. The detailed design of the YFP-ARF reporter construct is shown in **Figure 4B**.

Constructs syn-tas-cm*TAS*3 and ARF-YFP, plus a construct expressing miR173 needed for triggering *TAS1c* processing (Montgomery et al. 2008), were cloned in *A. tumefaciens* and co-infiltrated in *N. benthamiana* leaves for transient expression analysis. The correct processing and accumulation of the *syn-tas*-cm*TAS*3 was validated by stem-loop qRT-PCR (Figure S4A). A construct

expressing an amiRNA targeting *GUS* transcripts (Carbonell and Daros, 2017) was used as negative control. Infiltrated leaves were analyzed at 2 days post infiltration (2 dpi) by confocal microscopy . The expression of the YFP-ARF reporter was suppressed in the leaves co-infiltrated with the syn-tasiRNA3 construct, while the leaves co-infiltrated with the control construct targeting GUS-transcripts showed typical fluorescence (**Figure 4C**). The observation that accumulation (estimated by qRT-PCR) of ARF-YFP transcripts decrease in silenced plants reinforces results obtained by confocal microscopy (Figure S4B). These results suggest that lack of expression of the YFP-ARF reporter co-infiltrated with the syn-tasiRNA3 construct is due to the tasiRNA-mediated degradation of its mRNA, hence validating ¨*in vivo*¨ the functional activity of tasiARF as negative regulator of ARF3 and ARF4 transcripts in melon.

Functional activity of stress-responsive tasiRNAs

To gain mechanistic insights into the regulatory role of tasiARF in response to stress, we analyzed the accumulation of the target transcripts in those stress situations in which *TAS3*-derived tasiRNAs (tasiARF) showed significant differential accumulation in response to stress.

To evaluate the effects of changing environments on tasiARF populations, we used our data previously obtained from pairwise comparisons of total sRNAs recovered from control and treated samples with the statistical testing method DESeq2 (Sanz-Carbonell et al. 2019). According to our established filtering criteria (log2FC $\geq$1 or $\leq$-1, FDR value <0.05, and base mean ≥5), tasiARF accumulation was significantly reduced in the melon plants exposed to cold treatment (for both *TAS3-L* and *TAS3-S* derived tasiRNAs) and HSVd infection (for *TAS3-S* derived tasiRNA) (**Table 1 and Table S4**). These results revealed that, in coincidence with the observed in other plants species (Moldovan et al. 2009, Katiyar et al. 2015, He et al. 2018), the biogenesis of *TAS3*-derived tasiRNAs is a process susceptible to be altered by adverse environmental conditions. Quantitative RT-PCR (qRT-PCR) assays revealed that the accumulation of ARF2, ARF3 and ARF4 transcripts is significantly increased in cold-treated and HSVd-infected plants, as expected for the functional negative

regulation of the *TAS3*-derived tasiARFs, whose accumulation decreases in the same conditions, on its predicted targets. (**Figure 5**).

Table 1: Detail of the expression values (estimated by DeSEQ analysis) of the *TAS3-S* derived tasiARF sequence in melon plants exposed to diverse biotic and abiotic stress conditions. Only LogFC values ≥1 or ≤-1 and FDR values <0.05 were considered as significant for *bona fide* stress-responsive tasiRNAs.

tasiRNA	stress	base-mean	Log2FC	FDR
TTTCTTGACCTTGCAAGTCCA	*drought*	16,053	-0,677	0,589
TTTCTTGACCTTGCAAGTCCA	*HSVd*	15,671	-1,762	0,012
TTTCTTGACCTTGCAAGTCCA	*cold*	16,961	-1,667	0,027
TTTCTTGACCTTGCAAGTCCA	*salinity*	18,479	-0,438	0,760
TTTCTTGACCTTGCAAGTCCA	*Mon*	21,531	0,036	0,999
TTTCTTGACCTTGCAAGTCCA	*Agro*	15,630	-0,788	0,694
TTTCTTGACCTTGCAAGTCCA	*Short day*	29,119	0,888	0,368

Discussion

SiRNAs have been shown to play important roles in developmental regulation and stress responses in plants. Genome-wide identification of diverse biogenesis-grouped members of the "*siRNA family*" in an increasing number of plant species may have a high impact in the investigation of the molecular basis of gene regulation in sRNA-mediated stress response (Banerjeeab et al. 2017, Li et al. 2017, Kumar et al. 2018). In this study, we used a computational approach to identify putative *TAS* loci in the melon genome. As consequence of a strict selective process, only two potential *TAS3* loci (*TAS-Cmel735* and *TAS-Cmel737)* were considered as robustly predicted and subjected to subsequent validation analysis.

To date, there are two families of *TAS3* loci described in plants, identified respectively as *TAS3*-short (*TAS3-S*) and TAS3-long (*TAS3-L*) (Xia et al., 2017). In *TAS3-L*, only the 3´miR390 target site is cleavable, generating two in-phase tasiARFs (Allen et al., 2005; Axtell et al., 2006). The 5´target site of *TAS3-L* is usually noncleavable (Axtell et al., 2006). In contrast, both miR390 target sites of *TAS3-S* are cleavable, and one unique tasiARF is generated. Interestingly, has

been described that both 5´ and 3´ processed ends can potentially generate phased siRNAs (Xia et al., 2015, Xia et al, 2017).

Our results evidenced that, in coincidence with the previously described in apple (Xia et al, 2012) and strawberry (Xia et al, 2015), melon plants possesses both *TAS3-L and TAS3-S* families that transcribes length and short transcripts respectively. Although, the *TAS3-S* family is not present in arabidopsis, is conserved in many other dicot species (Xia et al, 2015). The existence of *TAS3*-derived transcripts in melon was initially validated by RT-PCR amplification. The prediction of well-established miR390-target sites at two (at both 5´and 3´ region) positions of the *TAS3*-derived transcript and the precise determination of such AGO-mediated processing by degradome assays provided the first experimental evidences supporting the presence of a ¨*bona fide*¨ *TAS3-S* loci in melon. miRNA-mediated cleavage is considered to be an important and necessary aspect of tasiRNA biogenesis, not only for ensuring sRNA production in the proper register, but also to recruit RDR6 and SGS3 to the ncRNA transcript. Surprisingly, we were incapable to confirm by degradome assay the miR390-mediated processing of the 3` region of the *TAS3-L*. However the recovering of high levels of phased siRNAs derived from the longer family member suggest that in melon tasiARFs might be generated from a 3´ non-cleavable *TAS3-L* transcript. Although, we cannot exclude the possibility that sequences-remnants derived from the miR390-mediated processing of the *TAS3-L* transcripts were under-represented in our degradome data-set, this observation is coincident with the recently described in arabidopsis where a single non-cleavable miRNA hit was sufficient requirement for RDR6 recruitment and functional tasiRNA biogenesis (de Felippes et al, 2017).

It is well established that the miR390/TAS3-ARF pathway represents a highly conserved negative regulator of the mRNAs encoding AUXIN RESPONSE FACTORS (ARF) in plants (Xia et al. 2017). Consequently, the prediction (by psRNA target) and validation (by degradome assays) that *ARF2, ARF3* and *ARF4* transcripts in melon are targets for the *TAS3*-derived tasiRNAs (tasiARF), contributed to reinforce our initial prediction. Finally, the demonstration that, in heterologous transient expression assays, the *TAS3-S* tasiRNA is able to

negatively regulate "*in vivo*" the expression of a target-containing transcript, provides robust evidence supporting the regulatory role of the first *TAS* locus identified in melon.

Regarding its behavior in response to stress conditions, we observed a significant reduction of *TAS3*-derived tasiARF in response to cold treatment (for both *TAS3-L* and *TAS3-S* derived tasiRNAs) and Hop stunt viroid (HSVd) infection (for *TAS3-S* derived tasiRNA). Hence these results suggest that the biogenesis of *TAS3*-derived tasiRNAs in melon plants is a dynamic process susceptible to be influenced by environmental conditions. The recent description (Sanz-Carbonell et al. 2019) of the decreased accumulation of miR390 (the key component responsible for triggering *TAS3* processing) in the melon plants exposed to both cold and HSVd treatments provides further functional support to this notion.

In line with a more general viewpoint, the incidence of environmental cues in the *TAS3* processing reported herein agrees with previous results that have indicated a close interrelation between tasiARF accumulation and stress conditions in poplar (He et al. 2018), arabidopsis (Moldovan et al. 2009), and sorgum (Katiyar et al. 2015). Interestingly, the observation that the general tendency of the alterations at the tasiARF level (down-regulation) observed in melon plants exposed to cold and HSVd was contradictory to that described for the *TAS3* derived tasiRNAs in poplar plants exposed to saline conditions (where up-regulation of *TAS3*-derived tasiRNAs was reported). This suggests that similarly to that described for stress responsive miRNAs (Kumar, 2014), changes in the accumulation level of stress-responsive tasiRNAs might be stress- and/or specie-dependent.

As mentioned above, *TAS3*-derived tasiRNAs mediate the cleavage of the transcripts encoding ARFs factors. These proteins are key components of the auxin-signaling cascade and directly control the transcription of primary auxin-responsive genes (Guilfoyle and Hagen, 2007). The miR390/TAS3/ARFs module is functionally diverse and regulates multiple plant developmental processes, including leaf patterning and expansion, phase transition, initiation of the shoot meristem, and also plays an important role in root nodule symbiosis (Adenot et al. 2006, Fahlgren et al. 2006, Garcia et al. 2006, Marin et al. 2010, de Luis et al.

2012, Yifhar et al. 2012, Zhou et al. 2013, Li et al. 2014, Cabrera et al. 2016). However, recent studies have revealed that *TAS3*-regulated ARFs are involved in responses to adverse environmental conditions. For instance, it has been described that the miR390/*TAS3*/ARFs module is a key regulator of root growth in poplar subjected to salt stress via the modulation of the auxin pathway (He et al. 2018). In rice, *ARF16* has been related to phosphate starvation responses (Shen et al. 2013), while *ARF12* has been associated with phosphate homeostasis. *ARF* genes responsive to changes in water levels have been described in soybean (Wang et al. 2014). Finally, differential expression of *ARF* transcripts in response to diverse abiotic stress conditions was also reported in tea (Xu et al. 2016) and banana plants (Hu et al. 2015). However, the regulatory pathways underlying this phenomenon remain in a conundrum (He et al. 2018).

Given that in general tasiRNA-defective mutants exhibit accelerated vegetative phase-change phenotypes, it has been suggested that arabidopsis *TAS3*-derived tasiRNAs could be involved in the regulation (mediated by ARF) of developmental processes in leaves and flowers (Guilfoyle and Hagen, 2007). Considering that equivalent pathways might be regulated by ARFs in melon, it is reasonable to assume that the down-regulation of the *TAS3*-derived tasiRNA observed in cold-exposed and HSVd-infected plants might be related to the developmental alterations observed in plants growing under these adverse environmental conditions, mainly characterized by delayed growth (Hataya et al. 2017, Hou et al. 2018). However, we cannot exclude the possibility that changes in the ARF levels observed in cold exposed and HSVd-infected plants may be also modulated, at least in part, by and stress-related increasing in its transcription level, resembling the previously observed in divers plant species such as rice (Jain and Khurana, 2009), sorghum (Wang et al, 2010), banana (Hu et al, 2015) and peper (Yu et al, 2017). Further functional evidence, which is difficult to obtain in melon, is necessary to experimentally support this hypothesis. Altogether, our results support that in coincidence with the previously described in arabidopsis (Hsieh et al. 2009, Luo et al. 2012) and tomato (Wu et al. 2017), tasiRNAs could emerge as potential modulators of the plant-environment interactions in melon plants.

Materials and methods

Sequence data

The sRNA sequence data used herein were obtained from 24 (three replicates by each treatment) previously described (Sanz-Carbonell et al. 2019). cDNA libraries obtained for control and stress-treated -*i*) abiotic agents: cold, drought, salinity, short day; *ii*) biotic agents: Hop stunt viroid (HSVd), *Monosporascus cannonballus and Agrobacterium tumefaciens*- melon plants (***Table S5***). The sequence data are publicly available in the SRA genomic repository of NCBI (BioProject IDPRJNA491809).

The statistical testing method DESeq2 v.1.18.1 (Love et al. 2014, https://bioconductor.org/packages/release/bioc/html/DESeq2.html] was used to evaluate the differential expression of the siRNAs in melon plants under stress conditions. Only the sRNAs with: i) log2-fold change (log2FC) ≥1 or ≤-1 for biological significance, ii) FDR value <0.05, and iii) base mean ≥5, which is the mean of normalized counts of all samples were considered as differentially expressed.

Identification of TAS candidate genes

In order to detect phased tasiRNAs in melon, the *TASI-PREDICTION* tool (http://srna-workbench.cmp.uea.ac.uk/tasi-prediction) was used with default parameters on previously described sRNA libraries obtained from melon plants (Sanz-Carbonell et al. 2019) and from melon genome sequences (Version 3.5.1) downloaded from https://www.melonomics.net. Predicted *TAS* regions were then aligned against known *TAS* sequences described for *Viridiplantae* in the NCBI database (https://www.ncbi.nlm.nih.gov) by command-line interface (Rstudio) using BLAST+ (https://www.ncbi.nlm.nih.gov/guide/howto/run-blast-local). Only sequences with homology levels ≥70% and minimum length alignment of 30 nt were considered as potential *TAS* precursors. The sequence corresponding to the *TAS3* gene identified in melon was deposited in the NCBI gene database with the accession number MK410640.

qRT-PCR assays

Total RNA was extracted from pooled leaves (~0.1 g) recovered from the treated and control melon plants using the TRI reagent (Sigma) according to the

manufacturer's instructions. To analyze target expression, total RNA (1.5 µg) extracted from control or treated plants was subjected to DNase treatment (EN0525, Thermo Scientific™) followed by reverse transcription using RevertAid First Strand cDNA Synthesis Kit (Thermo Scientific™) according to the manufacturer´s instructions by using of oligo-dT. Then, real-time PCR was performed (by triplicate) as previously described (Bustamante et al., 2018). The efficiency of PCR amplification was derived from a standard curve generated by four 5-fold serial dilution points of cDNA mixed from the two samples. Relative RNA expression was determined by using the comparative ΔΔCT method (Livak and Schmittgen, 2001) and normalized to the geometric mean of PROFILIN (NM001297545.1) and ADP-ribosylation factor-like (XM_008463181.2) expression, as reference control. Quantification of *syn-tas-cmTAS3* and miRNAs was performed starting from low-molecular weight RNA (< 200 nt) fractions obtained as described previously (Sanz-Carbonell et al., 2019). A slightly modified stem-loop-specific reverse transcription protocol for miRNAs detection (Czimmerer et al. 2013) was performed as previously described (Sanz-Carbonell et al., 2019). Primers used are listed in Table S6.

Degradome assay

Data of AGO-processed sequences used in this work were recovered from degradome libraries obtained from melon plants (Sanz-Carbonell et al. 2019).

Cloning and vectors construction

The syn-tasiRNA construct syn-tas-cm*TAS*3 was generated by annealing oligos AC-154 (ATTATCTTGACCTTGTAAGACCCAA) and AC-155 (GTTCTTGGGTCTTACAAGGTCAAGA), obtained with the P-SAMS website tool (Fahlgren et al. 2016), and by ligating the resultant insert into *pMDC32B-AtTAS1c-B/c* (Addgene plasmid #51773) as previously described (Carbonell et al. 2014). Constructs amiR-GUS and miR173 have been generated and used in previous works (Montgomery et al. 2008, Carbonell and Daros, 2017).

The ARF-YFP reporter is constituted by an ARF sequence (derived from both ARF3 and ARF4) predicted as target for the *TAS3*-derived tasiRNA (tasiARF), fused to the 3' end of the sequence encoding for the yellow fluorescent protein

(YFP) and cloned in a binary plasmid pMOG800 under the control of the Cauliflower mosaic virus 35S promoter and the *A. tumefaciens* nopaline synthase terminator (t-Nos) (Knoester et al. 1998). This construct was generated by amplifying the YFP-cDNA with a forward primer that includes an *Nco*I recognition site (GGTCTCCCATGGATGGTGAGCAAGGGCGA) and a reverse primer that contains the ARF sequence and an *Nhe*I recognition site (GGTCTCGCTAGCTCTTGACCTTGCAAGACCTTATCACTTGTACAGCTCGC C). The PCR amplified DNA was digested with *Nco*I and *Nhe*I and ligated into a linearized pMOG800 vector. A non-modified 35S-YFP-tNos construct was used as agro-infiltration-control.

Agro-infiltration assays

Nicotiana benthamiana leaves of 3-4 week-old plants were agroinfiltrated with the corresponding cultures of *A. tumefaciens* strain C58C1, previously transformed with the construct to be analyzed. The overnight grown bacterial culture was diluted in infiltration buffer (0.1 M MES, 1 M $MgCl_2$) up to an optical density at 600 nm (OD600) of 0.2 and injected on the abaxial side of the leaves using a 1 ml needle-less syringe (Gomez and Pallas, 2007). Agroinfiltrated plants were analyzed two days post-agroinfiltration. The growing conditions were as follow: photoperiod of 16 h under visible light (wavelength between 400-700 nm) with an irradiance of 65-85 $\mu mol \cdot m^{-2} s^{1}$ and 8 h of darkness; temperature cycles of 25 °C (light) and 18 °C (darkness) and relative humidity of 60-65 % (light) and 95-100 % (darkness). YFP fluorescence was observed using an inverted Zeiss LSM 780 confocal microscope and ZEN software (Carl Zeiss). Leaf dishes were cut and mounted in water. Then images were acquired using an objective plan-apochromat 40x/1.4 Oil DIC M27 (0.5 cm diameter).

Funding

This work was supported by Grants AGL2016-79825-R, BIO2014-61826-EXP (GG) from the Spanish Ministry of Economy and Competitiveness and BIO2017-83184-R (JAD)

from the Spanish Ministerio de Ciencia, Innovación y Universidades (co-financed FEDER funds).

Acknowledgments
J.M. was the recipient of a predoctoral contract from the ACIF programme (ACIF-2017-114) of the Conselleria d'Educació, Investigació, Cultura i Esport Generalitat Valenciana. A.C. was the recipient of a postdoctoral contract from the Ramón y Cajal programme (RYC-2017-21648) from the Ministerio de Ciencia, Innovación y Universidades (Spain).

Author contribution
LCS: performed experiments (related to tasiRNA identification and characterization) and analyzed results. MCM: performed experiments, analized and discussed the results. ASC: performed computational analysis. JMM: performed experiments (cloning and confocal microscopy observations). AC: designed the cloning strategy and contribute to wrote the main manuscript text. JAD: analyzed and discussed the results. GG: designed the experiments, discussed the results, prepared figures, and wrote the main manuscript text. All the authors revised the manuscript.

Disclosures:

Ethics approval and consent to participate
Not applicable

Consent to publish
Not applicable

Availability of data and materials
The datasets used and/or analyzed during the present study are available the genomic repository of NCBI with the following accession numbers (SRA - BioProject IDPRJNA491809 and MK410640) for sRNAs and the TAS sequence respectively.

Competing interests
The author(s) declare no competing interests.

REFERENCES

Adenot X., Elmayan T., Lauressergues D., Boutet S., Bouché N., Gasciolli V., Vaucheret H. (2006) DRB4-dependent TAS3 trans-acting siRNAs control leaf morphology through AGO7. *Curr. Biol.* 16: 927-932.

Allen E., Howell M.D. (2010) miRNAs in the biogenesis of trans-acting siRNAs in higher plants. *Semin. Cell Dev. Biol.* 21: 798-804.

Allen E., Xie Z., Gustafson, Carrington J.C. (2005) MicroRNA-directed phasing during trans-acting siRNA biogenesis in A.M. plants. *Cell* 121: 207-221.

Arif M.A., Fattash I., Ma Z., Cho S.H., Beike A.K., Reski R., Axtell M.J., Frank W. (2012) DICER-LIKE3 activity in Physcomitrella patens DICER-LIKE4 mutants causes severe developmental dysfunction and sterility. *Mol. Plant* 5: 1281-1294.

Axtell M.J. (2013) Classification and Comparison of Small RNAs from Plants. *Annu. Rev. Plant Biol.* 64: 137-159.

Axtell M.J., Jan C., Rajagopalan R., Bartel D.P. (2006) A two-hit trigger for siRNA biogenesis in plants. *Cell* 127: 565-577.

Banerjeeab S., Sirohi A., Ansaric A., Gillb S. (2017) Role of small RNAs in abiotic stress responses in plants. *Plant Gene* 11: 180-189.

Bielach A., Hrtyan M., Tognetti V.B. (2017) Plants under Stress: Involvement of Auxin and Cytokinin. *Int. J. Mol. Sci.* 4: 18(7).

Bologna N.G., Voinnet O. (2014) The diversity, biogenesis, and activities of endogenous silencing small RNAs in Arabidopsis. *Annu. Rev. Plant Biol.* 65: 473-503.

Borges F., Martienssen R. A., (2015) The expanding world of small RNAs in plants. *Nat. Rev. Mol. Cell Biol.* 16: 727-741.

Bustamante A., Marques M.C., Sanz-Carbonell A., Mulet J.M., Gomez G. (2018) Alternative processing of its precursor is related to miR319 decreasing in melon plants exposed to cold. *Sci. Rep.* 8: 15538.

Cabrera J., Barcala M., García A., Rio-Machín A., Medina C., Jaubert-Possamai S., Favery B., Maizel A., Ruiz-Ferrer V., Fenoll C., Escobar C. (2016) Differentially expressed small RNAs in Arabidopsis galls formed by Meloidogyne javanica: a functional role for miR390 and its TAS3-derived tasiRNAs. *New Phytol.* 209: 1625-1640.

Calanca P.P. (2017) Effects of abiotic stress in crop production, In M. Ahmed (Eds.), Quantification of climate variability, adaptation and mitigation for agricultural sustainability, New York, Springer, pp. 165180.

Carbonell A. (2017) Plant ARGONAUTEs: Features, Functions, and Unknowns. Methods Mol. Biol. 1640: 1-21.

Carbonell A., Daros J.A. (2017) Artificial microRNAs and synthetic trans-acting small interfering RNAs interfere with viroid infection. *Mol. Plant Pathol.* 18: 746-753.

Carbonell, Takeda A., Fahlgren N., Johnson S., Cuperus J., Carrington J.C. (2014) New Generation of Artificial MicroRNA and Synthetic Trans-Acting Small Interfering RNA Vectors for Efficient Gene Silencing in Arabidopsis. *Plant Physiol.* 165: 15-29.

Chitwood D.H., Nogueira F.T., Howell M.D., Montgomery T.A., Carrington J.C., Timmermans M.C. (2009) Pattern formation via small RNA mobility. *Genes Dev.* 23: 549-554.

Czimmerer Z., Hulvely J., Simandi Z., Varallyay E., Havelda Z., Szabo E., Balint B.L. (2013) A Versatile Method to Design Stem-Loop Primer-Based Quantitative PCR Assays for Detecting Small Regulatory RNA Molecules. *PLoS ONE*, **8**(1), e55168

Clepet C., Joobeur T., Zheng Y., Jublot D., Huang M., Truniger V., Boualem A., Hernandez-Gonzalez M.E., Dolcet-Sanjuan R., Portnoy V., Mascarell-Creus A., Caño-Delgado A., Katzir N., Bendahmane A., Giovannoni J.J., Aranda M.A., Garcia-Mas J., Fei Z. (2011) Analysis of expressed sequence tags generated from full-length enriched cDNA libraries of melon. *BMC Genomics* 12: 252.

D'Ario M., Griffiths-Jones S., Kim M. (2017) Small RNAs: Big Impact on Plant Development. *Trends Plant Sci.* 22: 1056-1068.

Dai X., Zhaohong-Zhuang Z., Zhao P., (2018) psRNATarget: a plant small RNA target analysis server (2017 release). *Nucleic Acids Res.* 46: W49-W54.

de Felippes F.F., Marchais A., Sarazin A., Oberlin S., Voinnet O. (2017) A single miR390 targeting event is sufficient for triggering TAS3-tasiRNA biogenesis in Arabidopsis. *Nucleic Acids Res.* 45: 5539-5554.

De Luis A., Markmann K., Cognat V., Holt D.B., Charpentier M., Parniske M., Stougaard J., Voinnet O. (2012) Two microRNAs linked to nodule infection and nitrogen-fixing ability in the legume Lotus japonicus. *Plant Physiol.* 160: 2137-2154.

Pingchuan Deng P., Muhammad S., Cao M., Wu L (2018). Biogenesis and regulatory hierarchy of phased small interfering RNAs in plants. *Plant Biotech. J.* 16: 965-975.

Fahlgren N., Hill S.T., Carrington J.C., Carbonell A. (2016) P-SAMS: a web site for plant artificial microRNA and synthetic trans-acting small interfering RNA design. *Bioinformatics* 32: 157-158.

Fahlgren N., Montgomery T.A., Howell M.D., Allen E., Dvorak S.K., Alexander A.L., Carrington J.C. (2006) Regulation of AUXIN RESPONSE FACTOR3 by TAS3 ta-siRNA affects developmental timing and patterning in Arabidopsis. *Curr. Biol.* 16: 939-944.

Fei Q., Xia R., Meyers B. (2013) Phased, Secondary, Small Interfering RNAs in Posttranscriptional Regulatory Networks. *Plant Cell* 25: 2400-2415.

Fukunaga R., Doudna J.A. (2009) dsRNA with 5 overhangs contributes to endogenous and antiviral RNA silencing pathways in plants. *EMBO J.* 28: 545-555.

Garcia D., Collier S.A., Byrne M.E., Martienssen R.A. (2006) Specification of leaf polarity in Arabidopsis via the trans-acting siRNA pathway. *Curr. Biol.* 16: 933-938.

Garcia-Mas J., Benjak A., Sanseverino W., Bourgeois M., Mir G., González V., Hénaff E., Câmara F., Cozzuto L., Lowy E., Alioto T., Capella-Gutiérrez S., Blanca J., Cañizares J., Ziarsolo P., Gonzalez-Ibeas D., Rodríguez-Moreno L., Droege M., Du L., Alvarez-Tejado M., Lorente-Galdos B., Melé M., Yang L., Weng Y., Navarro A., Marques-Bonet T., Aranda M., Nuez F., Picó B., Gabaldón T., Roma G., Guigó R., Casacuberta J., Arús P., Puigdomènech R. (2012) The genome of melon (*Cucumis melo* L.). *Proc. Natl. Acad. Sci.* USA 109: 11872-11877.

Gómez G., Pallás V. (2007) Mature monomeric forms of Hop stunt viroid resist RNA silencing in transgenic plants. *Plant J.* 51: 1041-1049.

González M., Xu M., Esteras C., Roig C., Monforte A.J., Troadec C., Pujol M., Nuez F., Bendahmane A., Garcia-Mas J., Picó B. (2011) Towards a TILLING platform for functional genomics in Piel de Sapo melons. *BMC Res. Notes* 4: 289.

Gonzalez-Ibeas D., Blanca J., Donaire L., Saladié M., Mascarell-Creus A., Cano-Delgado A., Garcia-Mas J., Llave C., Aranda M.A. (2011) Analysis of the melon (*Cucumis melo*) small RNAome by high-throughput pyrosequencing. *BMC Genomics* 12: 393.

Guilfoyle T.J., Hagen G. (2007) Auxin response factors. *Curr. Opin. Plant Biol.* 10: 453-460.

Hataya T., Tsushima T., Sano T. (2017) Hop Stunt Viroid in Viroids and Satellites. A. Hadidi, R. Flores, J.W. Randles, P. Palukaitis editors. Academic Press, Elsevier, pp. 199-210.

He F., Xu C., Fu X., Shen Y., Guo L., Leng M., Luo K. (2018) The MicroRNA390/TRANS-ACTING SHORT INTERFERING RNA3 Module Mediates Lateral Root Growth under Salt Stress via the Auxin Pathway. *Plant Physiol.* 177: 775-791.

Heisel S.E., Zhang Y., Allen E., Guo L., Reynolds T.L., Yang X., Kovalic D., Roberts J.K. (2018) Characterization of unique small RNA populations from rice grain. *PLoS One* 3: e2871.

Hou J., Zhou Y.F., Gao L.Y., Wang Y.L., Yang L.M., Zhu H.Y., Wang J.M., Zhao S.J., Ma C.S., Sun S.R., Hu J.B. (2018) Dissecting the Genetic Architecture of Melon Chilling Tolerance at the Seedling Stage by Association Mapping and Identification of the Elite Alleles. *Front. Plant Sci.* 9: 1577.

Howell M.D., Fahlgren N., Chapman E.J., Cumbie J.S., Sullivan C.M., Givan S.A., Kasschau K.D., Carrington J.C. (2007) Genome-wide analysis of the RNA-DEPENDENT

RNA POLYMERASE6/DICER-LIKE4 pathway in Arabidopsis reveals dependency on miRNA- and tasiRNA-directed targeting. *Plant Cell* 19: 926-942.

Hsieh L., Lin S., Shih A., Chen J., Lin W., Tseng C., Li W., Chiou T. (2009) Uncovering Small RNA-Mediated Responses to Phosphate Deficiency in Arabidopsis by Deep Sequencing. *Plant Physiol.* 151: 2120-2132.

Hu W., Zuo J., Hou X., Yan Y., Wei Y., Liu J., Li M., Xu B., Jin Z. (2015) The auxin response factor gene family in banana: genome-wide identification and expression analyses during development, ripening, and abiotic stress. *Front. Plant Sci.* 6: 742.

Islam W., Qasim M., Noman A., Adnan M., Tayyab M., Farooq T.H., Wei H., Wang L. (2018) Plant microRNAs: Front line players against invading pathogens. *Microb. Patholog.* 18: 9-17.

Johnson C., Kasprzewska A., Tennessen K., Fernandes J., Nan G., Walbot V., Sundaresan V., Vance V., Bowman L.H. (2009) Clusters and superclusters of phased small RNAs in the developing inflorescence of rice. *Genome Res.* 19: 1429-1440.

Katiyar A., Smita S., Muthusamy S.K., Chinnusamy V., Pandey D.M., Bansal K.C. (2015) Identification of novel drought-responsive microRNAs and trans-acting siRNAs from Sorghum bicolor (L.) Moench by high-throughput sequencing analysis. *Front. Plant Sci.* 6: 506.

Knoester M., van Loon L.C., van den Heuvel J., Hennig J., Bol J.F., Linthorst H. (1998) Ethylene-insensitive tobacco lacks nonhost resistance against soil-bornefungi. *Proc. Natl. Acad. Sci.* USA 95: 1933-1937.

Kumar R. (2014) Role of microRNAs in biotic and abiotic stress responses in crop plants. *Appl. Biochem. Biotech.* 174: 93-115.

Kumar V., Khare T., Shriram V., Shabir H., Wani S. (2018) Plant small RNAs: the essential epigenetic regulators of gene expression for salt-stress responses and tolerance. *Plant Cell Rep.* 37: 61-75.

Li F., Pignatta D., Bendix C., Brunkard J., MCohn J., Tung J., Sun H., Kumar P., Baker B. (2012) MicroRNA regulation of plant innate immune receptors. *Proc. Natl. Acad. Sci.* USA 109: 1790-1795.

Li S., Castillo-González C., Yu B., Zhang X. (2017) The functions of plant small RNAs in development and in stress responses. *Plant J.* 90: 654-670.

Li X., Lei M., Yan Z., Wang Q., Chen A., Sun J., Luo D., Wang Y. (2014) The REL3-mediated TAS3 ta-siRNA pathway integrates auxin and ethylene signaling to regulate nodulation in Lotus japonicus. *New Phytol.* 201: 531-544.

Livak K.J., Schmittgen T.D. (2001) Analysis of relative gene expression data using real-time quantitative PCR and the 2 -ΔΔCT method. *Methods* 25: 402-408.

Love M.I., Huber W., Anders S. (2014) Moderated estimation of fold change and dispersion for RNA-seq data with DESeq-2. *Genome Biol.* 15: 550.

Luo Q.J., Mittal A., Jia F., Rock C.D. (2012) An autoregulatory feedback loop involving PAP1 and TAS4 in response to sugars in Arabidopsis. *Plant Mol. Biol.* 80: 117-129.

Marin E., Jouannet V., Herz A., Lokerse A.S., Weijers D., Vaucheret H., Nussaume L., Crespi M.D., Maizel A. (2010) MiR390, Arabidopsis TAS3 tasiRNAs, and their AUXIN RESPONSE FACTOR targets define an autoregulatory network quantitatively regulating lateral root growth. *Plant Cell* 22: 1104-1117.

Martinez G., Köhler C. (2017) Role of small RNAs in epigenetic reprogramming during plant sexual reproduction. *Curr. Opin. Plant Biol.* 36: 22-28.

Mi S., Cai T., Hu Y., Chen Y., Hodges E., Ni F., Wu L., Li S., Zhou H., Long C., Chen S., Hannon G.J., Qi Y. (2008) Sorting of small RNAs into Arabidopsis argonaute complexes is directed by the 5' terminal nucleotide. *Cell* 133: 116-127.

Moldovan D., Spriggs A., Yang J., Pogson B.J., Dennis E.S., Wilson I.W. (2009) Hypoxia-responsive microRNAs and trans-acting small interfering RNAs in Arabidopsis. *J. Exp. Bot.* 61: 165-177.

Montgomery T.A., Howell M.D., Cuperus J.T., Li D., Hansen J.E., Alexander A.L., Chapman E.J., Fahlgren N., Allen E., Carrington J.C. (2008) Specificity of ARGONAUTE7-miR390 interaction and dual functionality in TAS3 trans-acting siRNA formation. *Cell* 133: 128-141.

Montgomery T.A., Yoo S.J., Fahlgren N., Gilbert S.D., Howell M.D., Sullivan C.M., Alexander A., Nguyen G., Allen E., Ahn J.H., Carrington J.C. (2008) AGO1-miR173 complex initiates phased siRNA formation in plants. *Proc. Natl. Acad. Sci.* USA 105: 20055-20062.

Ruggieri V., Alexiou K., Morata J., Argyris J., Pujol M., Yano R., Nonaka S., Ezura H., Latrasse D., Boualem A., Benhamed M., Bendahmane A., Aiese-Cigliano R., Sanseverino W., Puigdomènech P., Casacuberta J.M., Garcia-Mas J. (2018) An improved assembly and annotation of the melon (*Cucumis melo* L.) reference genome. *Sci. Rep*. 8: 8088.

Sanz-Carbonell A., Marques M.C., Bustamante, Fares M., Rodrigo G., Gomez G. (2019) Inferring the miRNA-mediated regulatory network of response to stress in melon. *BMC Plant Biol.* 19: 78.

Shen C., Wang S., Zhang S., Xu Y., Qian Q., Y. Qi, Jiang D.A. (2013) OsARF16, a transcription factor, is required for auxin and phosphate starvation response in rice (Oryza sativa L.). *Plant Cell Environ*. 36 (2013) 607-620.

Shriram V., Kumar V., Devarumath R.M., Khare T.S., Wani S.H. (2016) MicroRNAs as Potential Targets for Abiotic Stress Tolerance in Plants. *Front. Plant Scie.* 7: 817.

Sunkar R., Chinnusamy V., Zhu J., Zhu J.H. (2007) Small RNAs as big players in plant abiotic stress responses and nutrient deprivation. *Trends Plant Sci.* 12: 301-309.

Sunkar R., Li Y.F., Jagadeeswaran G. (2012) Functions of microRNAs in plant stress responses. *Trends Plant Sci.* 17: 196-203.

Takeda A., Iwasaki S., Watanabe T., Utsumi M., Watanabe Y. (2008) The mechanism selecting the guide strand from small RNA duplexes is different among argonaute proteins. *Plant Cell Physiol.* 49: 493-500.

Talmor-Neiman M., Stav, Klipcan L., Buxdorf K., Baulcombe D.C., Arazi T. (2006) Identification of trans-acting R. siRNAs in moss and an RNA-dependent RNA polymerase required for their biogenesis. *Plant J.* 48: 511-521.

Wang S., Zhang S., Sun C., Xu Y., Chen Y., Yu C., Qian Q., Jiang D., Qi Y. (2014) Auxin response factor (OsARF12), a novel regulator for phosphate homeostasis in rice (Oryza sativa). *New Phytol.* 201: 91-103.

Wei S., Wang L., Zhang Y., Huang D. (2013) Identification of early response genes to salt stress in roots of melon (*Cucumis melo* L.) seedlings. *Mol. Biol. Rep.* 40: 2915-2926.

Williams L., Carles C.C., Osmont K.S., Fletcher J.C. (2005) A database analysis method identifies an endogenous trans-acting short-interfering RNA that targets the Arabidopsis ARF2, ARF3, and ARF4 genes. *Proc. Natl. Acad. Sci.* USA 102: 9703-9708

Wu F., Chen Y., Tian X., Zhu X., Jin W. (2017) Genome-wide identification and characterization of phased small interfering RNA genes in response to Botrytis cinerea infection in Solanum lycopersicum. *Sci. Rep.* 7: 3019.

Wu S., Zhang B., Keyhaninejad N., Rodríguez G., Kim H., Chakrabarti M., Illa-Berenguer E., Taitano N., Gonzalo M., Díaz A., Pan Y., Leisner C., Halterman D., Buell C., Weng Y., Jansky S., van Eck H., Willemsen J., Monforte A., Meulia T., van der Knaap E. 82018) A common genetic mechanism underlies morphological diversity in fruits and other plant organs. *Nat. Commun.* 9: 4734.

Xia R., Xu J., Meyers B.C. (2017) The Emergence, Evolution, and Diversification of the miR390-TAS3-ARF Pathway in Land Plants. *Plant Cell* 29: 1232-1247.

Xia R., Zhu H., An Y.G., Beers E.P, Liu Z. (2012) Apple miRNAs and tasiRNAs with novel regulatory networks. Genome Biol. 13:R47

Xia R., Ye S., Liu Z., Meyers B.C., Liu Z. (2015) Novel and Recently Evolved MicroRNA Clusters Regulate Expansive F-BOX Gene Networks through Phased Small Interfering RNAs in Wild Diploid Strawberry. *Plant Physiol.* 169: 594-610.

Xu Y.X., Mao J., Chen W., Qian T.T., Liu S.C., Hao W.J., Li C.F., Chen L. (2016) Identification and expression profiling of the auxin response factors (ARFs) in the tea plant (Camellia sinensis (L.) O. Kuntze) under various abiotic stresses. *Plant Physiol. Biochem.* 98: 46-56.

Yang T., Wang Y., Teotia S., Zhang, Tang G. (2018) The Making of Leaves: How Small RNA Networks Modulate Leaf Development. *Front. Plant Sci.* 9: 824.

Yifhar T., Pekker I., Peled D., Friedlander G., Pistunov A., Sabban M., Wachsman G., Alvarez J.P., Amsellem Z., Eshed Y. (2012) Failure of the tomato trans-acting short interfering RNA program to regulate AUXIN RESPONSE FACTOR3 and ARF4 underlies the wiry leaf syndrome. *Plant Cell* 24: 3575-3589.

Yu Q., Liu Y., Li M., Yu B. (2017) Small RNA Biogenesis and Degradation in Plants. In: Rajewsky N., Jurga S., Barciszewski J. (eds) Plant Epigenetics. RNA Technologies. Springer. pp. 107-127.

Zhang B. (2015) MicroRNAs: a new target for improving plant tolerance to abiotic stress. *J. Exp. Bot.* 66: 1749-1761.

Zhang C., Li G., Wang J., Fang J. (2015) Identification of trans-acting siRNAs and their regulatory cascades in grapevine. *Bioinformatics* 28: 2561-2568.

Zhang X., Niu D., Carbonell A., Wang A., Lee A., Tun V., Wang Z., Carrington J.C., Chang C.E., Jin H. (2014) ARGONAUTE PIWIdomain and microRNA duplex structure regulate small RNA sorting in Arabidopsis. *Nat. Commun.* 5: 5468.

Zhou C., Han L., Fu C., Wen J., Cheng X., Nakashima J., Ma J., Tang Y., Tan Y., Tadege M., Mysore K.S., Xia G., Wang Z.Y. (2013) The trans-acting short interfering RNA3 pathway and no apical meristem antagonistically regulate leaf margin development and lateral organ separation, as revealed by analysis of an argonaute7/lobed leaflet1 mutant in Medicago truncatula. *Plant Cell* 25: 4845-4862.

Zhu H., Hu F., Wang R., Zhou X., Sze S.H., Liou L.W., Barefoot A., Dickman M., Zhang X. (2011) Arabidopsis Argonaute10 specifically sequesters miR166/165 to regulate shoot apical meristem development. *Cell* 145: 242-256.

Zhu J.K. (2016) Abiotic stress signaling and responses in plants. *Cell* 167: 313-324.

Jain M., Khurana J.P. (2009). Transcript profiling reveals diverse roles of auxin-responsive genes during reproductive development and abiotic stress in rice. *FEBS J.* 276: 3148-3162. [

Wang S.K., Bai Y.H., Shen C.J., Wu Y.R., Zhang S.N., Jiang D.A., Guilfoyle T.J., Chen M., Qi Y.H. (2010) Auxin-related gene families in abiotic stress response in Sorghum bicolor. *Funct. Integr. Genom.* 10: 533-546.

Hu W., Zuo J., Hou X., Yan Y., Wei Y., Liu J., Li M., Xu B., Jin Z. (2015) The auxin response factor gene family in banana: Genome-wide identification and expression analyses during development, ripening, and abiotic stress. *Front. Plant. Sci.* 6: 742.

Yu C., Zhan Y., Feng X., Huang Z.A., Sun C. (2017) Identification and Expression Profiling of the Auxin Response Factors in Capsicum annuum L. under Abiotic Stress and Hormone Treatments. Int J Mol Sci. 18(12): E2719.

FIGURE LEGENDS:

Figure 1: The predicted melon *TAS3-S* transcript is sliced by miR390. A) Graphic representation (not to scale) of the potential *TAS3-S* transcript (*TAS-CmeI735*) identified in the melon genome. The region position in chromosome 11 is also detailed. The miR390 target sites predicted by *psRNA-targets* tool are marked with gray arrows. miR390 sequence is shown in gray. The complementary sequence identified in *TAS3* transcripts is denoted magenta. **B)** Graphic representation of the miR390-cleaved *TAS3-S* transcripts detected by high-scale degradome assay. The obtained sequences were plotted (allowing 100% homologous matching) onto the *TAS3* sequence. The red lines on the X-axis indicate the position of the predicted miRNA recognition site in the melon *TAS3* transcript. The values on the Y-axis represent the number of obtained reads (normalized in reads per million).

Figure 2: Phased tasiRNAs arising from the melon *TAS3* transcripts. A) Read abundance distribution of *TAS3*-derived sRNAs in melon. 21 nt in length sRNAs (recovered from control libraries) were plotted (allowing 100% homologous matching) onto *TAS3* region in melon genome. Arrows indicate miR390 target sites. The X-axis represents a double-stranded *PHAS* locus. The reads abundance is represented in reads per million (RPM). **B)** Schematic representation of the processing inferred for the *TAS3*-S precursor in melon. miR390 target sites in the 3´region is marked. Phased 21 nt in length *TAS3-S* derived tasi-RNAs predicted computationally and recovered by sequencing are represented. The position of the tasiRNA identified as a negative modulator of ARF-transcripts (tasiARF) is highlighted at the position 5'D6[+] and its sequence detailed. **C)** Phased 21 nt in length derived from the miR390-guided processing it the 5´ region of the *TAS3-S* transcript predicted computationally and recovered by sequencing are represented. Radar plots show percentages of 21-nt reads corresponding to each one of the 21 registers from *TAS3-S* transcripts, with position 1 designated as immediately after the miR390-guided predicted cleavage site in the 5´region.

Figure 3: ARF family members are recognized as targets for *TAS3* tasiRNA activity in melon. Graphic representation of tasiRNA-cleaved *ARF3*, *ARF4* and *ARF2* melon transcripts detected by degradome assay. The obtained sequences were plotted (allowing 100% homologous matching) onto the *ARF3* (XM017043883.1), *ARF4* (XM008465701) and *ARF2* (XM-008466144) sequences. The red lines on the X-axis show the position of the predicted tasiRNA target sites. The values on the Y-axis represent the number of obtained reads (normalized in reads per million, RPM). The tasiARF sequence is denoted in magenta. The complementary sequences identified in target transcripts are presented in gray.

Figure 4: The *TAS3*-derived tasiARF trigger AGO-mediated processing of target-transcripts *in vivo*. A and B) Physical map (not to scale) of the constructs used herein. The miR173 and tasiARF target sites are detailed. miR173 and tasi-ARF sequences are

denoted in blue and magenta, respectively. The Cauliflower mosaic virus 35S promoter and the nopaline synthase terminator (t-Nos) are also represented. **C)** *N. benthamiana* plants were co-infiltrated with agrobacterium transformed with *i*) YFP-ARF reporter plus amiR-GUS and amiR173, and *ii*) YFP-ARF reporter plus syn-tas-cmTAS3 as control. As observed in the lower panels, the YFP-ARF reporter expression is clearly reduced compared to control (middle panels), when is co-expressed with the syn-tasiRNA and the amiR173 constructs. The unmodified YFP (upper panels) was used as YFP expression control. R1 to R3 are replicates of the same experiments in different *N. benthamiana* plants.

Figure 5: The ARF2, ARF3 and ARF4 expression correlate to the changes in the accumulation of *TAS3*-derived tasiRNAs responsive to stress conditions. A) Histogram showing the means of the relative accumulation respect to the control samples (in Log of ΔΔCT value) of ARF3, ARF4 and ARF2 transcripts (gray bars) in melon plants exposed to cold treatment and HSVd-infection as estimated by qRT-PCR. Error bars show the confidence interval of the difference between means. The bars in magenta represent the accumulation levels (estimated by sRNA sequencing data analysis) (in LogFC) of the *TAS3*-derived tasiRNA in the correspondent melon samples. **B**) Detail of the data represented in A.

Table 1: Detail of the expression values (estimated by DeSEQ analysis) of the *TAS3*-S derived tasiARF sequence in melon plants exposed to diverse biotic and abiotic stress conditions. Only LogFC values ≥1 or ≤-1 and FDR values <0.05 were considered as significant for "*bona fide"* stress-responsive tasiRNAs.

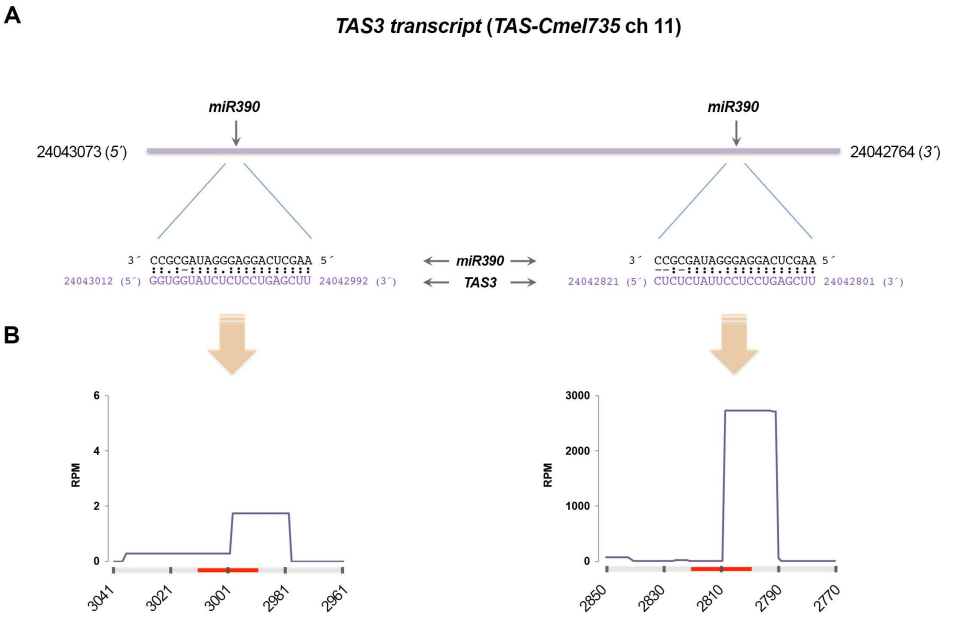

Figure 1: The predicted melon TAS3-S transcript is sliced by miR390. A) Graphic representation (not to scale) of the potential TAS3-S transcript (TAS-Cmel735) identified in the melon genome. The region position in chromosome 11 is also detailed. The miR390 target sites predicted by psRNA-targets tool are marked with gray arrows. miR390 sequence is shown in gray. The complementary sequence identified in TAS3 transcripts is denoted magenta. **B)** Graphic representation of the miR390-cleaved TAS3-S transcripts detected by high-scale degradome assay. The obtained sequences were plotted (allowing 100% homologous matching) onto the TAS3 sequence. The red lines on the X-axis indicate the position of the predicted miRNA recognition site in the melon TAS3 transcript. The values on the Y-axis represent the number of obtained reads (normalized in reads per million).

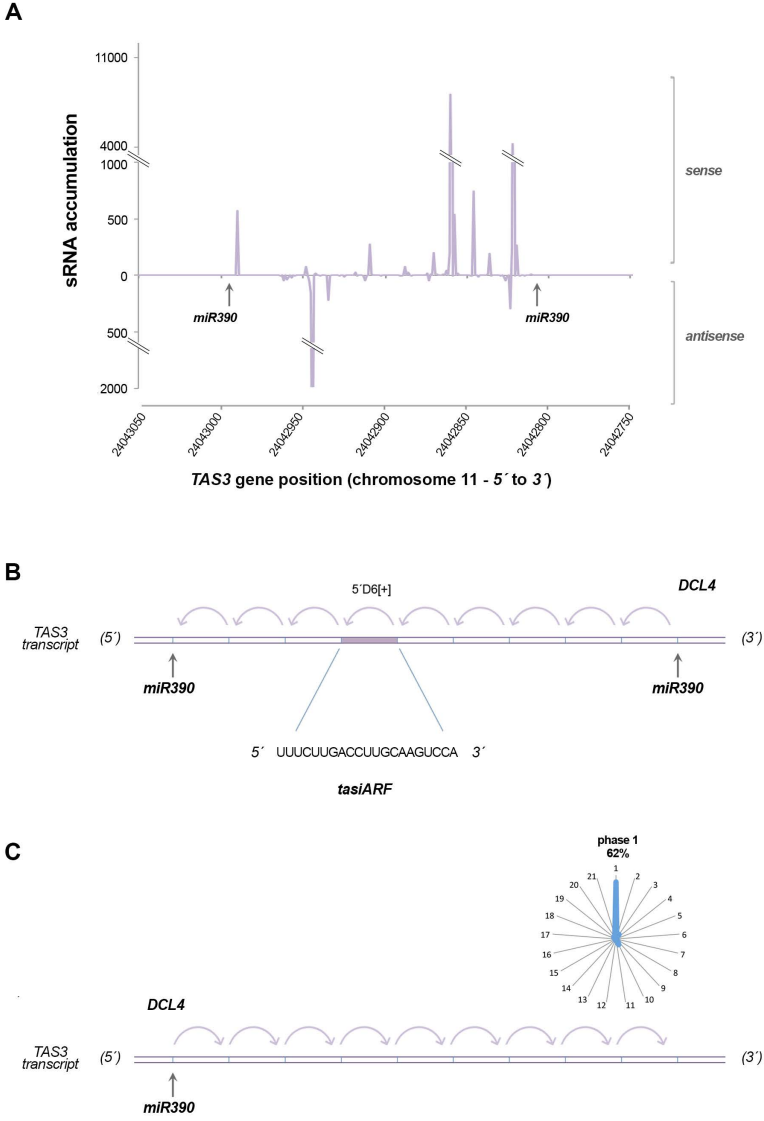

Figure 2: Phased tasiRNAs arising from the melon TAS3 transcripts. A) Read abundance distribution of TAS3-derived sRNAs in melon. 21 nt in length sRNAs (recovered from control libraries) were plotted (allowing 100% homologous matching) onto TAS3 region in melon genome. Arrows indicate miR390 target sites. The X-axis represents a double-stranded PHAS locus. The reads abundance is represented in reads per million (RPM). **B)** Schematic representation of the processing inferred for the TAS3-S precursor in melon. miR390 target sites in the 3´region is marked. Phased 21 nt in length TAS3-S derived tasi-RNAs predicted computationally and recovered by sequencing are represented. The position of the tasiRNA identified as a negative modulator of ARF-transcripts (tasiARF) is highlighted at the position 5'D6[+] and its sequence detailed. **C)** Phased 21 nt in length derived from the miR390-guided processing it the 5´ region of the TAS3-S transcript predicted computationally and recovered by sequencing are represented. Radar plots show percentages of 21-nt reads corresponding to each one of the 21 registers from TAS3-S transcripts, with position 1 designated as immediately after the miR390-guided predicted cleavage site in the 5´region.

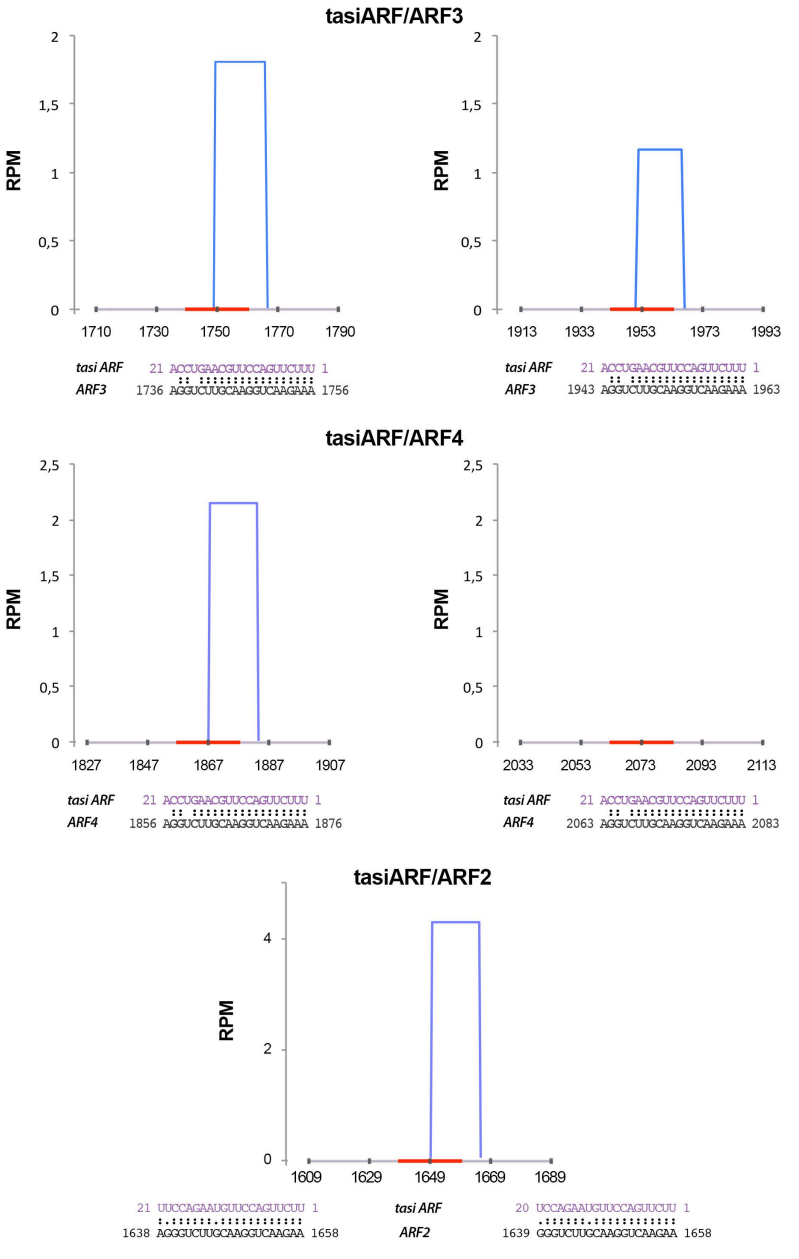

Figure 3: ARF family members are recognized as targets for TAS3 tasiRNA activity in melon. Graphic representation of tasiRNA-cleaved ARF3, ARF4 and ARF2 melon transcripts detected by degradome assay. The obtained sequences were plotted (allowing 100% homologous matching) onto the ARF3 (XM017043883.1), ARF4 (XM008465701) and ARF2 (XM-008466144) sequences. The red lines on the X-axis show the position of the predicted tasiRNA target sites. The values on the Y-axis represent the number of obtained reads (normalized in reads per million, RPM). The tasiARF sequence is denoted in magenta. The complementary sequences identified in target transcripts are presented in gray.

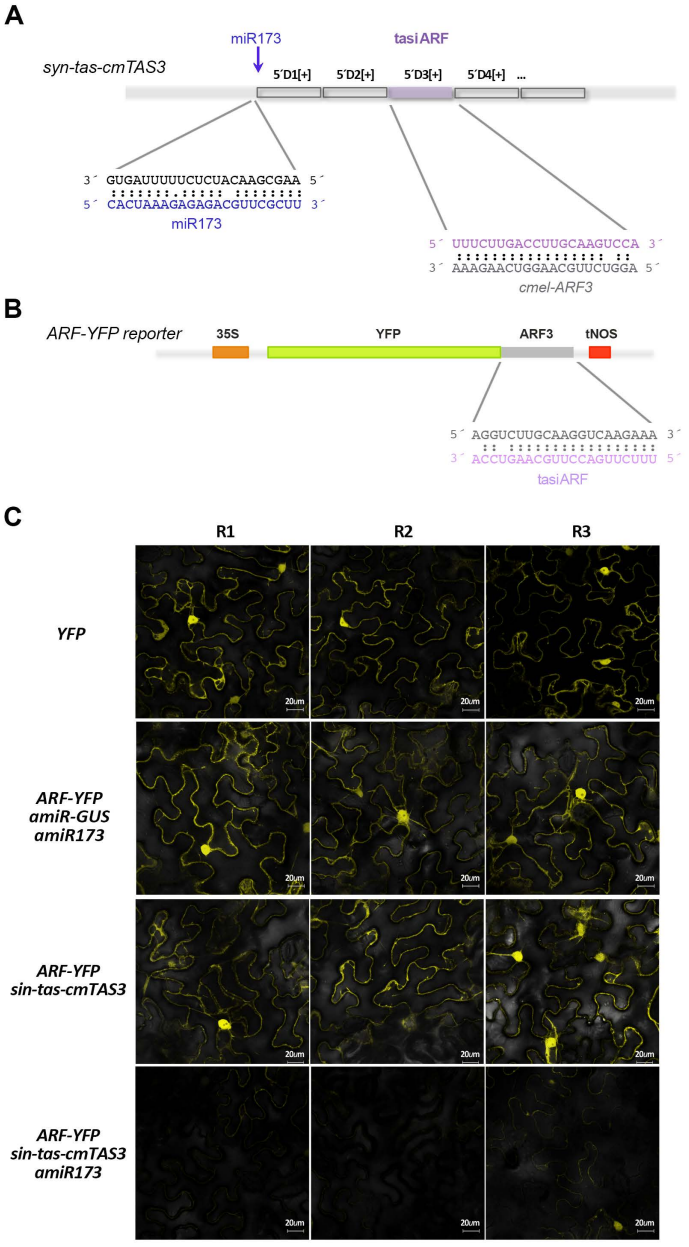

Figure 4: The TAS3-derived tasiARF trigger AGO-mediated processing of target-transcripts in vivo. A and B) Physical map (not to scale) of the constructs used herein. The miR173 and tasiARF target sites are detailed. miR173 and tasi-ARF sequences are denoted in blue and magenta, respectively. The Cauliflower mosaic virus 35S promoter and the nopaline synthase terminator (t-Nos) are also represented. **C)** N. benthamiana plants were co-infiltrated with agrobacterium transformed with i) YFP-ARF reporter plus amiR-GUS and amiR173, and ii) YFP-ARF reporter plus syn-tas-cmTAS3 as control. As observed in the lower panels, the YFP-ARF reporter expression is clearly reduced compared to control (middle panels), when is co-expressed with the syn-tasiRNA and the amiR173 constructs. The unmodified YFP (upper panels) was used as YFP expression control. R1 to R3 are replicates of the same experiments in different N. benthamiana plants.

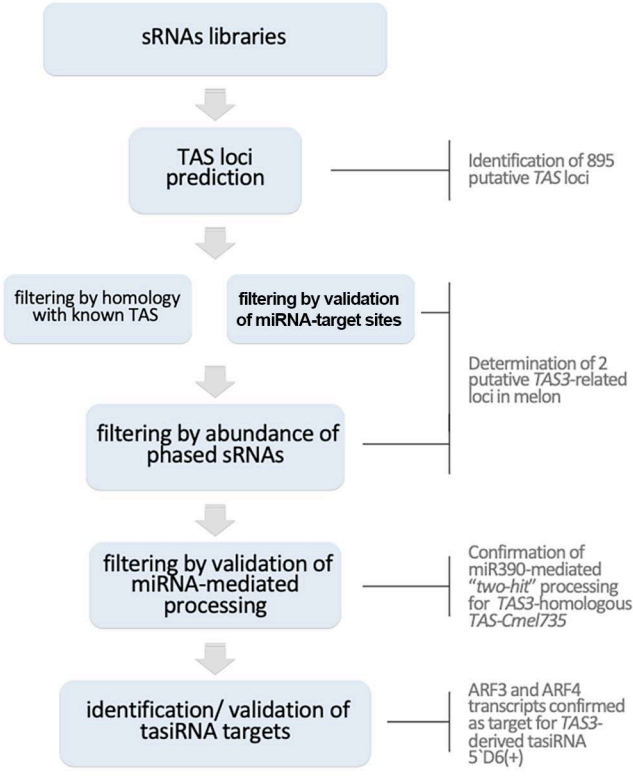

Figure S1: Graphic representation of the experimental approach used in this work to identify TAS-derived tasiRNAs in melon plants. In total 24 independent libraries were analysed. Putative TAS loci were filtered using three criteria: i) homology with known TAS genes ≥70%, ii) ≥5 phased sequences identified, and iii) validation of miRNA-mediated processing.

A

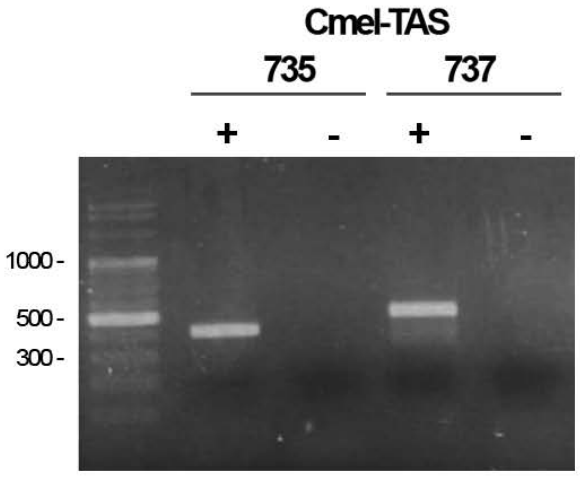

	PCR		
	oligo	position (chr 11)	fragment
Cmel-TAS735	TAS735-F1 5'-TTCTCACAAACCCTACGCTTCTACC- 3'	24043057 - 24043033	397 nt
	TAS735-R1 5'-CAACTCTTCAAAAATCCCATCACCATCG- 3'	24042660 - 24042687	
Cmel-TAS737	TAS737-F 5'-ACGACCAACCGACCCAACTG- 3'	28040984 - 28041003	502 nt
	TAS737-R1 5´-CGGTTTGCTTGCTCTTCTTGATCTTC- 3'	28041486 - 28041461	

B

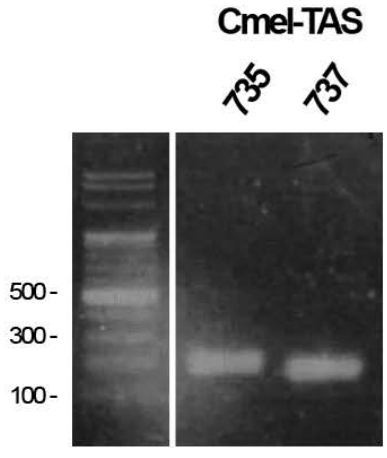

	RT-PCR		
	oligo	position (chr 11)	fragment
Cmel-TAS735	TAS735-F2 5'-GACTTCGTTCGTGGATGTTTTGTTTCC- 3'	24042848 - 24042822	188 nt
	TAS735-R1 5'-CAACTCTTCAAAAATCCCATCACCATCG- 3'	24042660 - 24042687	
Cmel-TAS737	TAS737-F 5'-ACGACCAACCGACCCAACTG- 3'	28040984 - 28041003	159 nt
	TAS737-R2 5'-GAGAAATAGAAACGGAAATAAGGAAG- 3'	28041143 - 28041118	

Figure S2: Electrophoresis in agarose-gels of the products obtained by specific amplification of predicted *CmTAS* gene by PCR **(A)** and their derived transcripts by RT-PCR **(B)**. Detailed description of the primers used in these assays is also provided.

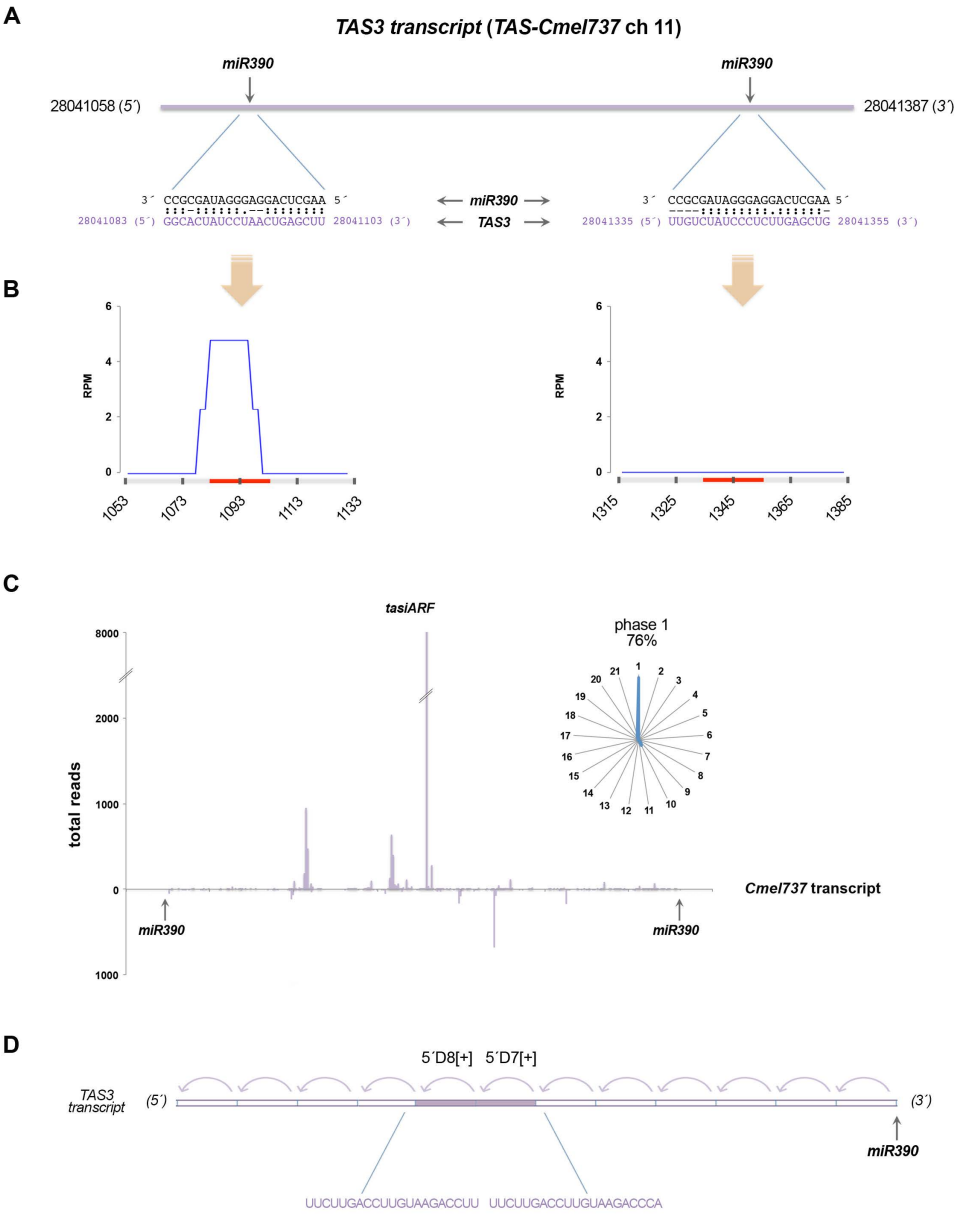

Figure S3: Predicted *TAS-Cmel737* is not sliced by miR390. A) Graphic representation (no at scale) of the *TAS-Cmel737* transcript identified in melon . Position in chromosome 11 is also detailed. Predicted miR390 target sites are marked with arrows. miR390 sequence and the complementary sequence identified in *TAS* transcript are detailed. **B)** Graphic representation of miR390-cleaved TAS transcripts detected by degradome assay. Sequences were plotted (allowing 100% homologous matching) onto the *TAS-Cmel737* sequence. Contrarily to the expected remnants derived from the canonical double cut of *TAS-Cmel737* guided by miR390 in both 5´ and 3´ regions were not recovered. Red lines on the X-axis indicate the position of the predicted miRNA recognition site in the TAS transcript. The values on the Y-axis represent the number of obtained reads (normalized in reads per million). **C)** Read abundance distribution of *TAS3-L* derived sRNAs in melon. 21 nt in length sRNAs (recovered from control libraries) were plotted (allowing 100% homologous matching) onto TAS3 region in melon genome. Arrows indicate predicted miR390 target sites. The X-axis represents a double-stranded PHAS locus. Radar plots show percentages of 21-nt reads corresponding to each one of the 21 registers from *TAS3-L* transcripts, with position 1 designated as immediately after the miR390-guided predicted cleavage site in the 3´region. **D)** Schematic representation of the processing inferred for the *TAS3-L* in melon. miR390 target site in the 3´region is marked. Phased 21 nt in length *TAS3-L* derived tasi-RNAs predicted computationally and recovered by sequencing are represented. The position of the tasiRNA identified as a negative modulator of ARF-transcripts (tasiARF) at the positions 5'D7[+] and 5'D8[+] is highlighted and its sequences detailed.

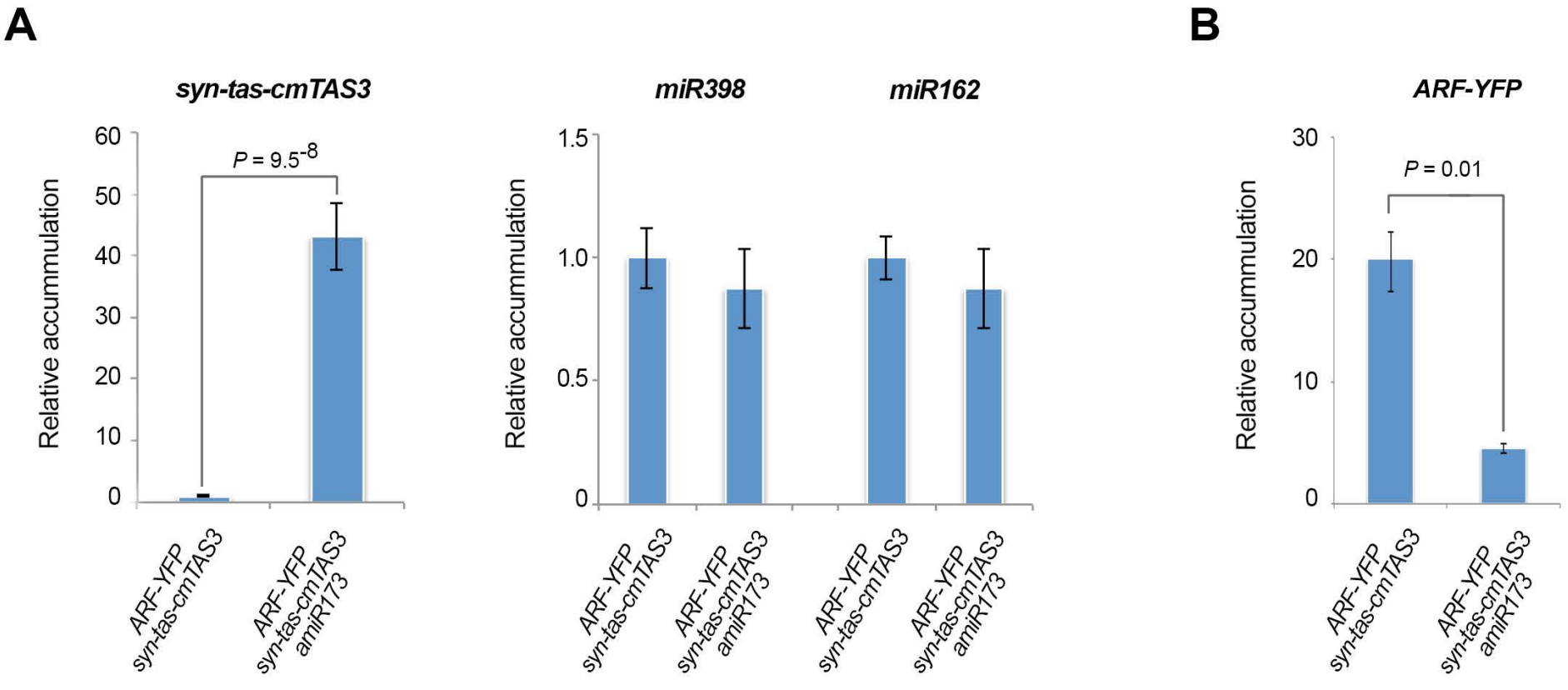

Figure S4: *sin-tas-cmTAS3* is highly accumulated in ARF-YFP silenced plants. A) (left pannel) Histogram showing the means of the relative accumulation (in Log of ΔΔCT value) respect to the control samples (without trigger amiR173 construct) transcripts as estimated by stem-loop qRT-PCR. Right) relative accumulation of endogenous miR398 and miR162 used as internal controls. Error bars show the confidence interval of the difference between means. B) Relative accumulation of ARF-YFP transcripts in silenced plants co-expressing *syn-tas-cmTAS3* and amiR173 constructs.